THE EVOLUTION OF LINE-TIED CORONAL ARCADES INCLUDING A CONVERGING FOOTPOINT MOTION

B. INHESTER*, J. BIRN, and M. HESSE

Space Plasma Physics Group, Los Alamos National Laboratory, Los Alamos, NM 87545, U.S.A.

(Received 9 July, 1991; in revised form 12 October, 1991)

Abstract. It has been demonstrated in the past that single, two-dimensional coronal arcades are very unlikely driven unstable by a simple shear of the photospheric footpoints of the magnetic field lines. By means of two-dimensional, time-dependent MHD simulations, we present evidence that a resistive instability can result if in addition to the footpoint shear a slow motion of the footpoints towards the photospheric neutral line is included. Unlike the model recently proposed by van Ballegooijen and Martens (1989), the photospheric footpoint velocity in our model is nonsingular and the shear dominates everywhere. Starting from a planar potential field geometry for the arcade, we find that after some time a current sheet is formed which is unstable with respect to the tearing instability. The time of its onset scales with the logarithm of the magnetic diffusivity assumed in our calculation. In its nonlinear phase, a quasi-stationary situation arises in the vicinity of the x-line with an almost constant reconnection rate. The height of the x-line above the photosphere and the distance of the separatrix footpoints remain almost constant in this phase, while the helical flux tube, formed above the neutral line, continuously grows in size.

1. Introduction

The forced motion of the photospheric footpoints of closed coronal magnetic field lines is widely considered to be the main energy source for the magnetic energy stored in the corona and is believed to be ultimately responsible for the high coronal temperature and the X-ray emission from active regions (Parker, 1972, 1983). The average energy input into the corona by photospheric motions moving the line-tied magnetic field lines has been estimated by various authors to be of the order of 10^7 ergs s^{-1} cm^{-2} (Golub *et al.*, 1980; Parker, 1983).

While the energy supply by the random motion of the photospheric footpoints seems to be more or less continuous, its release from the corona is often observed to be intermittent and eruptive. Many energetic processes in the solar corona, like flares, prominence eruptions, and coronal mass ejections, set their energy free on time scales much shorter than the time necessary to supply the energy from the solar surface. The released energy often is a fair fraction of the magnetic energy present in the erupting volume of the corona (e.g., Forbes, 1990). For instance, for a coronal mass ejection with an energy of 10^{32} ergs (Howard *et al.*, 1985) released within minutes over an area of 10^{20} cm^2, the above estimate of the energy input by line-tied motions implies that it takes more than a day to accumulate the free energy in the magnetic field. This suggests that line-tied motions not only gradually enhance the magnetic energy in the corona, but eventually drive the magnetic field configuration into a situation where its equilibrium is lost or an instability occurs, the onset of which then is responsible for the rapid release

* Permanent address: Max-Planck-Institut für Aeronomie, D-411 Katlenburg-Lindau, Germany.

Solar Physics **138:** 257–281, 1992.

of at least part of the stored energy. As the speed of the footpoint motion in general is well below the coronal Alfvén velocity, the magnetic field configuration stays close to the equilibrium field associated with the actual footpoint position until nonequilibrium or an instability is reached.

Consequently, there have been quite a number of attempts to quantitatively model the formation of unstable magnetic field geometries starting from a simple, low-energy initial configuration. As most active regions are observed to occur near photospheric neutral lines, where the photospheric normal component of the magnetic field reverses its sign, an often adopted model for this low-energy initial configuration consists of plane, two-dimensional magnetic arcades. In almost all of these models, the footpoints are then sheared in the invariant direction along the photospheric neutral line. It turned out, however, that a shear of the footpoints alone, i.e., a displacement parallel to the photospheric neutral line, in a two-dimensional geometry is not enough to drive an initially simple magnetic arcade field configuration unstable (Klimchuk, Sturrock, and Yang, 1988; Biskamp and Welter, 1989). Other model calculations of eruptive or unstable processes therefore include some additional source of free energy like a localized, persistent (Zwingmann, 1987) or impulsive pressure source (e.g., Steinolfson and Hundhausen, 1988; Linker, van Hoven, and Schnack, 1990), or an externally fed coronal line current (Forbes, 1990). Some models already start off with an unstable magnetic field configuration (Forbes and Priest, 1983) or with an ensemble of magnetic arcades (Mikic, Barnes, and Schnack, 1988; Biskamp and Welter, 1989). However, there is no observational evidence for the presence of additional energy sources or of the presence of multiple magnetic arcades in active regions of the solar corona.

In the present paper, we demonstrate that it is indeed not necessary to invoke the above-mentioned additional energy sources to drive an initially stable, two-dimensional arcade magnetic field configuration towards an instability. The effect of line-tying is sufficient for that purpose if the footpoint motion includes besides the shear along the photospheric neutral line also a component of the photospheric boundary velocity that converges the footpoints towards the neutral line.

This kind of footpoint motion has also been considered in modelling the evolution of the coronal magnetic field by van Ballegooijen and Martens (1989). They proposed a model for the formation of filaments based on forced reconnection of field lines exactly at the photospheric neutral line. The reconnection rate in their model is entirely controlled by the photospheric velocity component towards the neutral line and the normal component of the photospheric magnetic flux density in its vicinity. In order to achieve a finite reconnection rate, however, they had to assume a singular convergent velocity component in the photosphere, the magnitude of which increases inversely proportional to the distance from the neutral line as the neutral line is approached.

Here, we consier instead a continuous, nonsingular footpoint motion whose speed is everywhere small compared to the shear velocity. Further details of our model are outlined in Section 2. Starting from a stable arcade magnetic field geometry, the velocity component towards the magnetic neutral line then helps to drive the system towards a resistive instability as is demonstrated in Section 3. The evolution of the system after

the tearing mode has set in is presented in Section 4, and relations to previous work and potential applications of our results to solar coronal phenomena are discussed in Section 5.

2. Model and Method

In our simulation model, we describe the coronal plasma by the isothermal MHD equations in two dimensions. The model is two-dimensional in the sense that gradients vanish in one invariant direction, whereas the components of all vector fields in this direction are self-consistently included. Such a model is also often called $2\frac{1}{2}$-dimensional. After a suitable normalization, based on a typical length scale L_0, density ρ_0, and magnetic field strength B_0, these equations can be written in conventional notation as

$$\frac{\partial \rho}{\partial t} = -\nabla \cdot \mathbf{u}\,, \tag{1a}$$

$$\frac{\partial \mathbf{u}}{\partial t} = -\nabla(p + \tfrac{1}{2}B^2) + \nabla \cdot (\mathbf{BB} - \mathbf{uv}) + \frac{1}{S_k}\nabla^2 u\,, \tag{1b}$$

$$\frac{\partial \mathbf{B}}{\partial t} = \nabla \cdot (\mathbf{Bv} - \mathbf{vB}) + \frac{1}{S_m}\nabla^2 \mathbf{B}\,, \tag{1c}$$

where

$$\mathbf{u} = \rho \mathbf{v}\,, \qquad p = \beta_0 \rho\,,$$

and $S_m = V_{A0}L_0/\eta$ is the conventional Lundquist number defined by the typical Alfvén speed $V_{A0} = B_0/\sqrt{\mu_0 \rho_0}$ and the magnetic diffusivity η. The velocity and the time have been normalized by the Alfvén speed V_{A0} and the Alfvén transit time L_0/V_{A0}, respectively, so that S_k corresponds to a kinematic Lundquist number where the magnetic diffusivity η is replaced by the kinematic viscosity ν of the plasma, or a modified Reynolds number normalized by V_{A0} rather than by the typical flow speed. Since we assume a constant temperature, the ratio of pressure and density is constant and corresponds in normalized variables to the ratio β_0 of the thermal and the magnetic pressure. In all the calculations presented, $\beta_0 = 0.1$ has been assumed.

In a two-dimensional geometry with $\hat{y}$ as the invariant direction all variables depend only on the x- and z-coordinates, and we can represent the poloidal magnetic field by a flux function A so that

$$\mathbf{B} = \hat{y} \times \nabla A + \hat{y} B_y\,. \tag{2}$$

Here, ∇ operates only in the x, z-plane and the contour lines of the flux function $A(x, z)$ represent the projection of the field lines onto the x, z-plane.

Since the photospheric footpoints are assumed to move slowly in our simulations, we expect our results to be most of the time close to a static equilibrium solution of (1), where $\mathbf{u} = 0$. In the ideal case $S_m = \infty$ this requires that p and B_y are constant along

the field lines (Birn and Schindler, 1981; Low, 1982),

$$p = p(A), \qquad B_y = B_y(A), \tag{3a}$$

and that the $\mathbf{j} \times \mathbf{B}$ force balances the pressure force which gives rise to

$$\Delta A = -\frac{\mathrm{d}}{\mathrm{d}A}\left(\tfrac{1}{2}B_y^2 + p\right). \tag{3b}$$

In fact, Mikic, Barnes, and Schnack (1988) and Biskamp and Welter (1989) have pointed out that solving the time-dependent problem (1) while insuring that the velocities remain small compared to the Alfvén speed is a convenient way to obtain a sequence of approximate solutions to the equilibrium problem (3b).

The typical values for normalization quantities L_0, ρ_0, and B_0 are imposed by the initial configuration of our model. The initial density is chosen to be homogeneously distributed over the computational domain with a value of ρ_0. The coronal magnetic field at $t = 0$ is assumed to be a potential field and corresponds to the field of a horizontally orientated line dipole of strength $B_0 L_0^2$ at a depth of L_0 below the photospheric plane at $z = 0$. The resulting field lines are thus circular arcades in the x, z-plane, bridging a photospheric neutral line in the y-direction at the origin $x = 0$, $z = 0$ of our computational plane. Similar initial magnetic field geometries have previously been used in analytical work by numerous authors (see the review by Birn and Schindler, 1981) and in two-dimensional MHD simulations by Zwingmann (1987), Klimchuk, Sturrock, and Yang (1988) and others.

The characteristic speed V_{A0} in our model corresponds to the Alfvén velocity at the origin of our coordinate system. At a finite height, however, there is a decrease of the Alfvén velocity due to the decrease in the magnetic field strength rather than an increase as in the real solar corona. This reversal of the Alfvén speed gradient does not have a great impact on the results of this calculation because we consider primarily processes that are slow compared to a typical Alfvén transit time.

Similarly, the model plasma β increases with height well above its value close to the photosphere, whih is approximately β_0. Since the important processes in our model occur just above the photosphere, the value of $\beta_0 = 0.1$ can be considered as the relevant magnitude of the plasma β in our simulation. The fact that β increases with height probably has a stabilizing effect on the calculation. Since the relevant β is small and transport of heat and radiation complicate the energy budget of the coronal plasma considerably, we will, as a first step, neglect adiabatic and other kinds of heating in our model and adopt an isothermal energy equation.

In the high-temperature, low-density corona the (compressional) kinematic viscosity ν is expected to be much larger than the magnetic diffusivity η (Priest, 1982). For a typical scale of 105 km, kinematic and magnetic Lundquist numbers of the order of 10^6 and 10^{14}, respectively, are obtained, which is beyond what can reliably be treated in computer simulations. In our calculations we assumed a value of $S_k = 1000$, while for S_m, various values were used. The results reported here were obtained with Lundquist numbers $S_m = 1000$ and $S_m = \infty$.

To solve Equations (1) numerically, we employ a leap-frog scheme which has almost no numerical diffusion except what is induced locally by a flux limiting procedure added after each time step. The numerical dispersion of the leap-frog code does not affect our results strongly since we want to simulate a system always close to its equilibrium rather than wave phenomena. A good compromise between the desire to have a high spatial resolution where necessary and a large computational domain at the expense of a moderate computation time was found by selecting a non-equidistant grid of 186×93 points in x and z with a grid size varying between $\Delta x = \Delta z = 0.006 L_0$ near the origin $x = 0, z = 0$, and $\Delta x = \Delta z = 0.06 L_0$ at the outer boundaries located at $x = \pm 3L_0$ and $z = 3L_0$, respectively.

The boundary condition along the outer boundaries includes a vanishing normal gradient of ρ and a vanishing of the tangential magnetic component B_y. The latter condition ensures that there is no current flow through the outer boundaries. For the other magnetic field components, $\nabla \cdot \mathbf{B} = 0$ and $\hat{y} \cdot \nabla \times \mathbf{B} = 0$ was used to determine the normal derivative of the normal and the second tangential component of **B**, respectively. On the photospheric boundary, $\nabla \cdot \mathbf{B} = 0$ is used again to determine the normal derivative of B_z. For ρ and the tangential components of **B**, the second normal derivative was chosen to vanish, which gave the numerically most stable results.

As boundary condition for the velocity we prescribe its tangential components and demand its normal component to vanish in the photospheric plane $z = 0$. An alternative boundary condition, allowing for photospheric influx, would fix the photospheric pressure and leave the velocity component parallel to the boundary magnetic field undetermined. However, it was found that this boundary condition results in a numerical instability, originating close to $x = 0, z = 0$, where the magnetic arcades become infinitesimally small. The more restrictive boundary condition that we have chosen instead probably increases the physical stability of the system (Zwingmann, 1987). On the top and side boundaries we assume all velocity components to vanish. Again, these are very restrictive conditions which tend to stabilize the system compared to the case where the boundaries are open or infinitely far away. Therefore, whenever an instability is obtained with our numerical set-up, the instability will crtainly show also under less restrictive but more realistic boundary conditions.

The boundary velocity prescribed in the photospheric plane includes a shear component antisymmetric with respect to the photospheric neutral line, similar to what has been considered in previous papers (Klimchuk, Sturrock, and Yang, 1988; Mikic, Barnes, and Schnack, 1988; Biskamp and Welter, 1989). However, we also include a converging footpoint motion towards the neutral line. We have tried several specific shapes for the footpoint velocity variation without essential differences in the results. For the case presented here, we have chosen

$$\mathbf{v}(x, z = 0) = \begin{bmatrix} -w_{x0} \\ w_{y0} \\ 0 \end{bmatrix} \left(\frac{x}{1 + \left(\frac{x}{0.5}\right)^2} - \frac{x}{1 + \left(\frac{3}{0.5}\right)^2} \right), \tag{4}$$

where the last term in the brackets causes $\mathbf{v}(x, z = 0)$ to vanish at the lateral boundaries $x = \pm 3$. The parameters w_{z0} and w_{y0} in (4) represent the velocity gradients of the x- and y-components, respectively, of the photospheric motion at the neutral line. They were chosen to be $w_{y0} = 0.20$ and $w_{x0} = 0.06$ or 0.0 for a comparison. These values result in maximum dimensionless velocity amplitudes of about 0.015 in the x- and 0.05 in the y-direction. This is well below the Alfvén velocity, which is of order unity or larger in dimensionless units. In Figure 1, we display the location of footpoints that initially

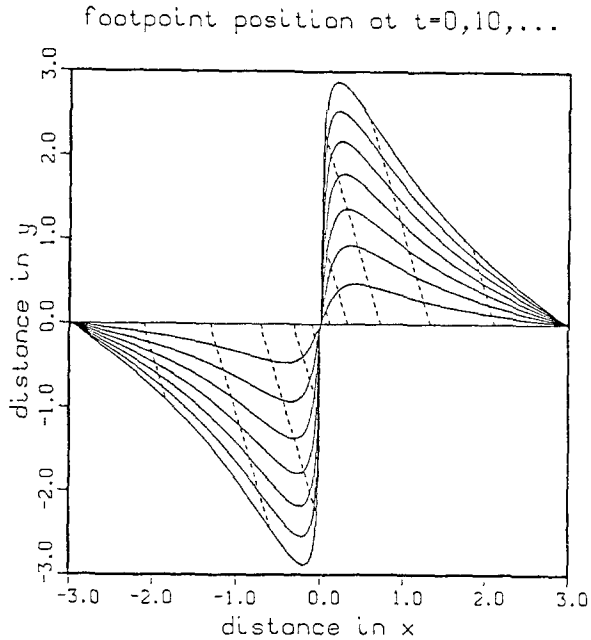

Fig. 1. Location of footpoints at $t = 0, 10, 20, \ldots, 70$ in the photospheric plane that at $t = 0$ form a straight line at $y = 0$. The footpoints are moved according to (4) with $w_{x0} = 0.06$, $w_{y0} = 0.2$. The dashed lines represent trajectories of individual footpoints starting from $y = 0$. These trajectories are straight because the ratio v_x/v_y is the same constant everywhere in the photospheric plane.

form a straight line $y = 0$ in the photospheric x, y-plane if they are moved according to (4).

Even though v_x is small compared to v_y, the convergent component of the footpoint motion makes a fundamental difference in the results of the simulation. In the next section, we therefore compare the simulation results obtained in the case of a simple shear with a case where v_x does not vanish.

3. Loss of Stability

It is not straightforward to see what changes a converging footpoint motion imposes on the coronal magnetic field configuration compared to a situation where the footpoints

of the field lines are only sheared. If there is no shear motion at all and we neglect the influence of the small plasma pressure for a moment, then if B_y vanishes and the field is a potential field initially, it remains so. In a low-β plasma, a shear therefore is necessary to enable the system to accumulate free energy beyond the energy of a potential field, which has the minimum energy for given boundary conditions. A shear of the footpoints alone, however, seems to be insufficient to drive a simple arcade unstable or towards a loss of equilibrium (Klimchuk, Sturrock, and Yang, 1988; Biskamp and Welter, 1989).

In Figure 2, we compare the evolution of the field-line projection onto the x, z-plane.

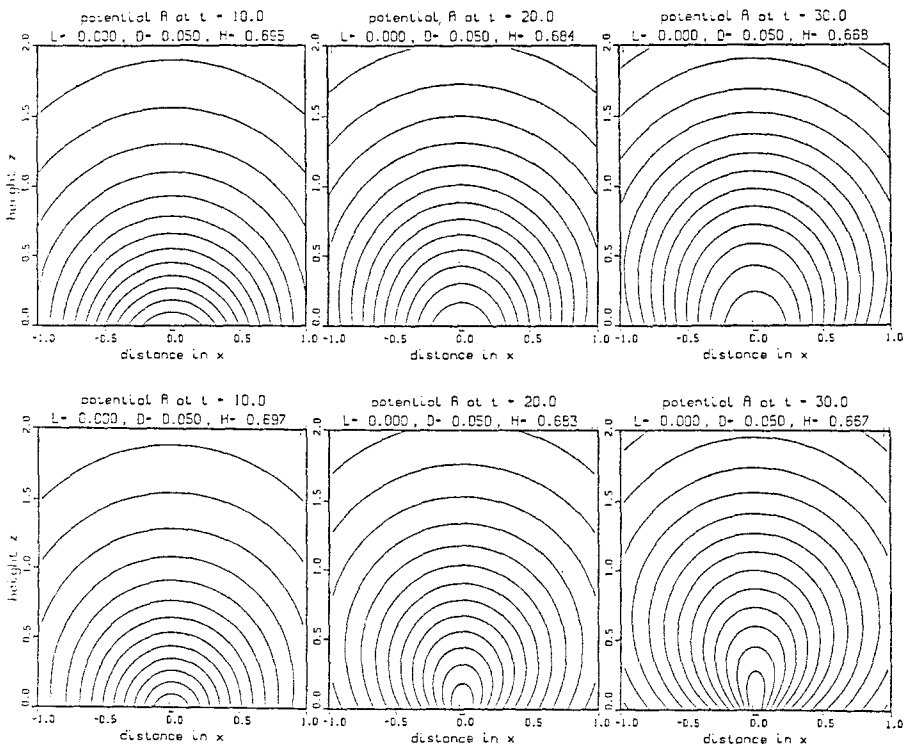

Fig. 2. Field lines projected into the x, z-plane for run A (top) and B (bottom). In run A, the footpoints were only sheared in the y-direction; in addition to the shear, run B includes a convergent component of the footpoint motion. Both cases were run with $S_m = \infty$. The poloidal magnetic flux per unit distance in the y-direction in between adjacent field lines is $\Delta A = 0.05$ in the dimensionless units.

According to (2), these are just the contour lines of the flux function A = const. Note that in our convention, $A = 0$ corresponds to the innermost field line close to the origin and the magnetic flux function A increases for the field lines further out until $A = 1$ for the field line at infinity. The longest field line that does not intercept the top or side boundaries of our computational domain corresponds to about $A = 0.75$.

In the sequence at the top of the figure the footpoints are only sheared according to (4) with $w_{x0} = 0$ (run A), the bottom sequence also includes a converging footpoint

motion (run B). The parameters of the two runs are otherwise identical and have $S_m = \infty$. By $t = 30$, an initially straight line in the photosphere along the $\hat{x}$-axis has been distorted so that it forms a shear angle of 80° and 86° with the $\hat{y}$-axis in run A and B, respectively. The results are only presented until $t = 30$, but run A without converging footpoints was continued until $t = 100$ without finding any instability or loss of equilibrium. By this time, the shear angle has increased to about 87°.

In both cases shown in Figure 2 the shear of the footpoints causes B_y to rise and the resulting increase in the magnetic pressure inflates the field lines. In equilibrium, the differential toroidal magnetic flux in the y-direction between two neighboring field lines projected into the x, z-plane is (e.g., Birn and Schindler, 1981)

$$B_y(A)V(A) = Y(A)\,, \tag{5}$$

where

$$V(A) = \int_{A = \text{const.}} \frac{\mathrm{d}l}{|\nabla A|} \tag{6}$$

is the associated differential flux-tube volume, i.e., the volume of a magnetic flux tube of unit flux, and $Y(A)$ is the total shear displacement parallel to the y-axis between the two footpoints of the closed field line on which the flux function has the value specified by the argument A. Note that the integration in (6) extends along the projection of the field line with A = const. in the x, z plane, so that $V(A)$ is also equivalent to the differential area between field-line projections in that plane.

At least intuitively, the inflation of the field lines can be understood by arguments given by Jockers (1976) and Sakurai (1989). As $Y(A)$ grows due to the shear motion, at first $B_y(A)$ rises while the projected field lines and, hence, $V(A)$ remain relatively unchanged. When a shear angle of about 45° is reached, the magnitude of $B_y(A)$ is of the order of the magnitude of ∇A. The requirement for a pressure balance (3b) prevents $B_y(A)$ to increase any further so that a continued enhancement of $Y(A)$ in (5) now causes primarily $V(A)$ to rise. In the two-dimensional projection, the length of a field line depends on the width of the flux tubes below so that $V(A)$ rises both by enhancing the length of the projected field lines and by pushing the field lines further apart.

In run B, the evolution is somewhat different because the field lines are also squeezed together due to the converging footpoint motion. One would, therefore, expect the field lines to rise somewhat faster in this case if $V(A)$ was to increase in the same way as in run A. From Figure 2, however, we find that the peak heights of related field lines in both runs are nearly identical. We conclude that in run B, the differential volume $V(A)$ does not increase as quickly as in run A, where the footpoints are not converged. Since the shear displacement $Y(A)$ at any given time is almost the same in both runs, B_y obviously continues to grow in run B, even after a shear angle of about 45° has been reached. This increase in B_y can be understood qualitatively because the resulting enhancement of the magnetic pressure gradient ∇B_y^2 compensates in the vertical direction the increased downward tension force which is due to the stronger curvature of

the field-line projections. In horizontal direction it balances the increased gradient of B_z^2.

Biskamp and Welter (1989) have demonstrated that in a sheared two-dimensional arcade, the component of the magnetic field along the shear direction evolves, after some time, selfsimilarly and they have suggested that this evolution is responsible for the stability of sheared arcades. In Figure 3(a), we recover this evolution of B_y for run A.

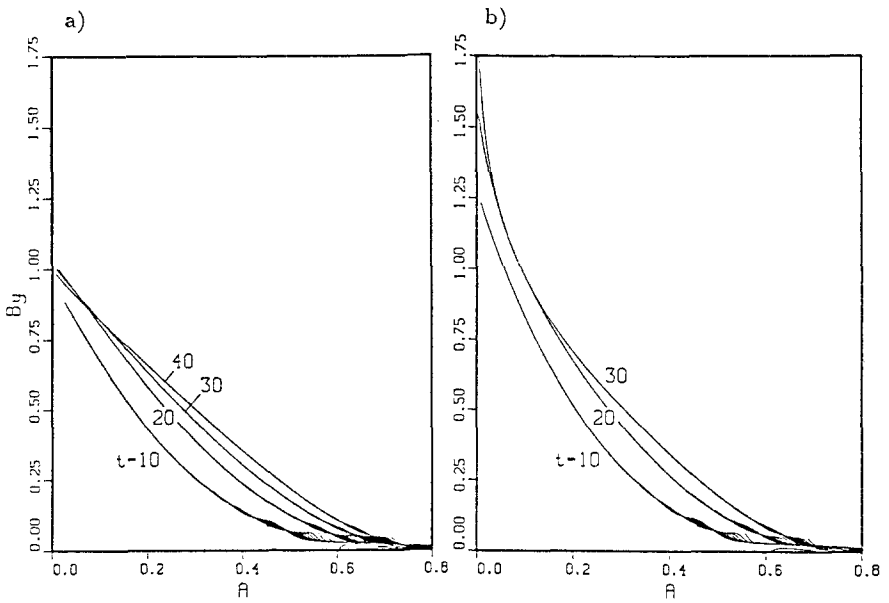

Fig. 3. Relation between B_y and the magnetic flux function A for run A (panel a) and run B (panel b). Note that A increases from $A = 0$ for the innermost loop of the arcade until $A \simeq 0.8$ for the outermost loop of the simulation box.

In this figure, the data points $B_y(A)$ from nearly all grid points of the two-dimensional simulation box are superimposed. For a given time, almost all these data points fall onto a single curve, which is evidence of the fact that the magnetic field configuration is very close to an equilibrium even though we employ a time-dependent code. Only on field lines with a large value of the flux function A some discrepancy from a unique relation $B_y(A)$ is seen, which stems from upward propagating waves launched by the sudden start of the photospheric shear motion at $t = 0$. As the time proceeds, B_y evolves in a self-similar manner in the sense that the relation between B_y and A for $t \geq 30$ becomes almost independent of time even though the field lines continue to rise and B_y accordingly undergoes temporal changes in space.

Furthermore, in run A without converging footpoints the time-asymptotic relation between B_y and the magnetic flux function A is close to linear. If we again neglect the small thermal pressure, this is equivalent to the formation of a force-free equilibrium

$\mathbf{j} = \alpha \mathbf{B}$ where, using (2) and (3b),

$$\alpha = \frac{j_y}{B_y} = \frac{\Delta A}{B_y} = -\frac{\partial}{\partial A} B_y$$

turns out to be a global constant. The same field configuration would arise for identical magnetic boundary conditions from a variational procedure in which the magnetic energy is minimized for a given total magnetic helicity of the system (Woltjer, 1958; Sakurai, 1979). The magnetic field configuration in run A therefore seems to automatically approach a state of minimum energy given the magnetic helicity imposed by the footpoint shear. As a resistive instability preferentially destroys magnetic energy rather than magnetic helicity (see, e.g., Berger, 1984), Biskamp and Welter (1989) concluded that the sheared arcade is probably stable with respect to such an instability.

The equivalent relation between toroidal magnetic field B_y and the value of the flux function A for run B is displayed in Figure 3(b). We note that $B_y(A)$ does not become time-independent nor does B_y approach a linear relationship with A. Especially for small values of the flux function A, that is, on the innermost loops of the arcade close to the origin, B_y continuously grows in time and $B_y(A)$ becomes strongly curved after $t \simeq 20$. The possibility of a resistive instability can, therefore, not be ruled out if the footpoints are not only sheared but are also converging towards the photospheric neutral line.

The differences between run A and B are most apparent in the evolution of the current densities. As discussed above, in run A without converging footpoints, $j_y = \alpha B_y(A)$ varies almost linearly with the flux function A after some time and its contour plot in Figure 4(a) therefore closely resembles the representation of the field line in Figure 2(a). This is different for run B with converging footpoints for which j_y is strongly concentrated on the innermost field lines. As a result, a thin current sheet is eventually formed that extends upwards from the photospheric neutral line (Figure 4(b)). Moreover, the spatial maximum of j_y increases almost exponentially with time in the latter case, while it settles to a constant value in case of run A (Figure 4(c)).

The growth of the current density is due to the converging footpoints and can roughly be understood on the basis of the following arguments. In the vicinity of $x = 0$, the footpoint motion in the x-direction is approximately

$$v_x(x, z = 0) \simeq -x w_{x0} \tag{7}$$

according to (4). The time it takes a point in the photosphere to be convected from its initial position x_0 to some x then is

$$t(x, x_0) = \int_{x_0}^{x} \frac{\mathrm{d}x'}{v_x(x')}$$

which yields after integration

$$x(t) \simeq x_0 \, e^{-w_{x0} t} . \tag{8}$$

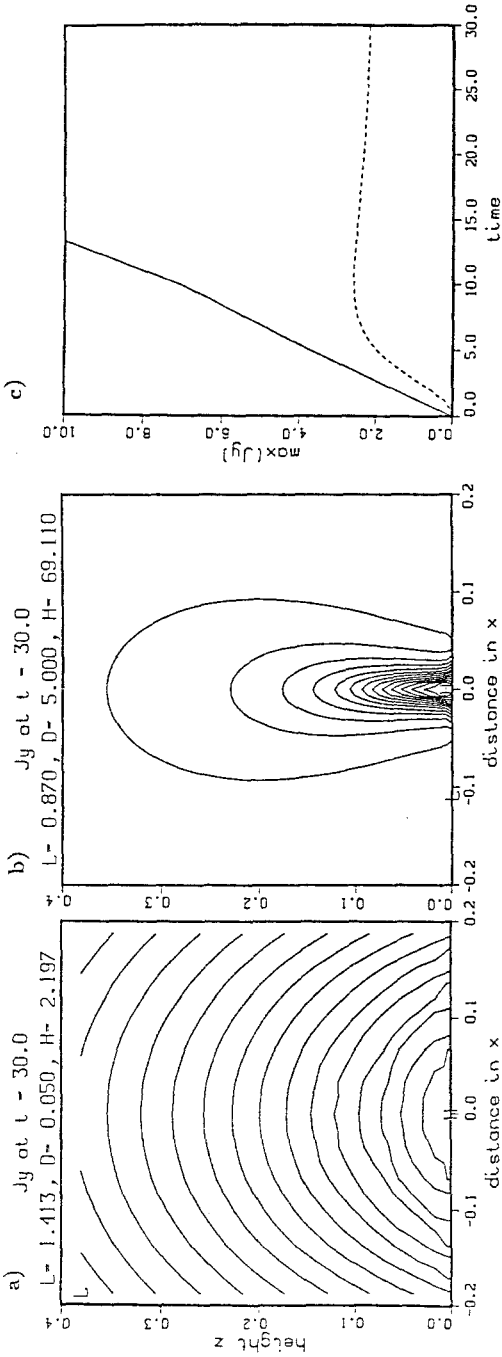

Fig. 4. Contour lines of j_y at $t = 30$ for run A (panel a) and run B (panel b). The spatial maximum of j_y is in both cases obtained at $x = 0$, $z = 0$ (marked by the letter H) with values of 2.197 and 69.11 in dimensionless units, respectively. The difference between the contour levels is $\Delta j_y = 0.05$ (a) and 5 (b) dimensionless units. (c) displays the temporal evolution of the spatial maximum value of j_y for run A (dashed) and run B (solid).

The values of the magnetic flux function A are simply convected in the photosphere so that for $x \simeq 0$

$$A(x, z = 0, t) = A(xe^{w_{x0}t}, z = 0, t = 0) .$$

Consequently, $B_z = \partial A/\partial x$ and $j_y \simeq \partial^2 A/(\partial x)^2$ increase roughly as $\exp(w_{x0}t)$ and $\exp(2w_{x0}t)$, respectively. Similarly, the width of the current sheet decreases approximately inversely proportional to the magnitude of B_z. By $t = 30$, the half width of the current sheet has dropped to $D \simeq 0.04$.

The compression of the current sheet indicates the possibility that the configuration becomes unstable to a resistive tearing mode. In Figure 5 we demonstrate that the

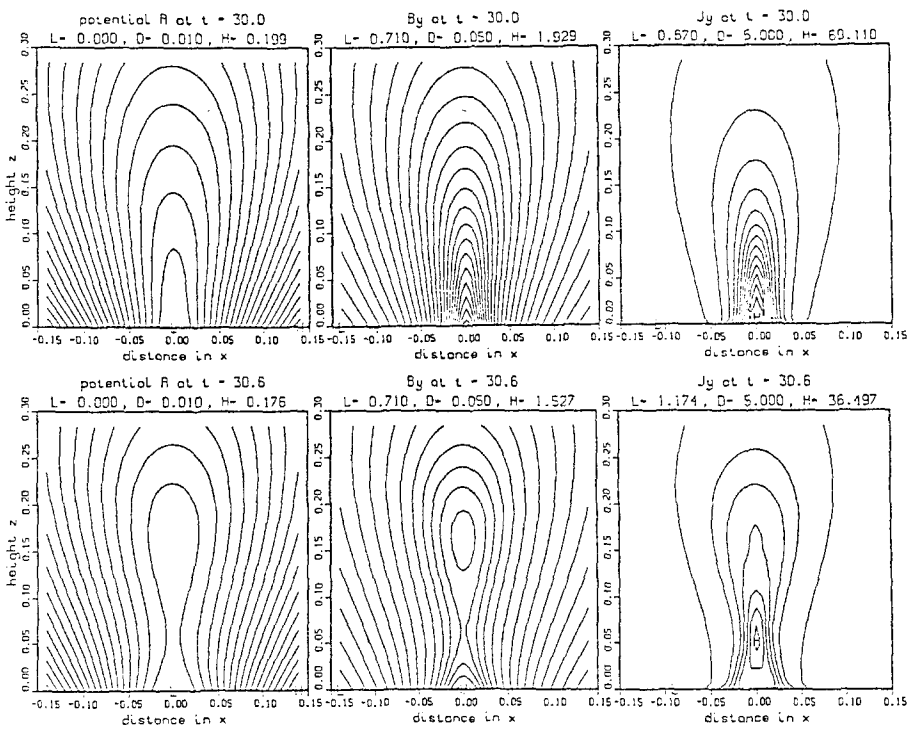

Fig. 5. Projected field lines (left column) and contours of B_y (center column) and j_y (right column) at $t = 30$ (top row) and $t = 30.6$ (bottom row). The configuration at $t = 30$ was obtained from run B without resistivity. At $t = 30$, a finite resistivity corresponding to $S_m = 1000$ was introduced, the velocity was reset to zero, and the footpoints were fixed at their momentary positions. The differences in the contour levels are $\Delta A = 0.01$ (left column), $\Delta B_y = 0.05$ (center column), and $\Delta j_y = 5$ (right column), respectively.

magnetic field configuration obtained at $t = 30$ in run B by the combined action of footpoint shear and convergence is indeed resistively unstable. For this purpose, we adopted the magnetic field and density at this instance as the initial configuration for a new run. Starting from a plasma at rest, the footpoints were kept fixed at their new initial position and a finite magnetic diffusivity corresponding to $S_m = 1000$ was

assumed to allow for a resistive instability to grow. While this run was performed primarily to test the resistive stability of the configuration, it can also be interpreted as simulating an actual evolution that has led to a point where a microinstability sets in and suddenly increases the effective resistivity to an anomalous value. A similar experiment starting from the magnetic field configuration of run A at $t = 30$ did, es expected, not show any signature of an instability.

The top row of Figure 5 shows **B** and j_y at the time the magnetic diffusivity was switched on. As can be seen in the bottom row of Figure 5, the typical characteristics of a tearing instability (Furth, Killeen, and Rosenbluth, 1963; White, 1983) become visible only 0.6 time units later: the formation of a magnetic x-line in the invariant y-direction at some height above the photosphere and the formation of a closed magnetic island above. This x-line is closely associated with a maximum of the current density j_y. In Figure 6 (a), the appreciable acceleration of the plasma into the region of the magnetic island is shown, which also is typical for the tearing mode.

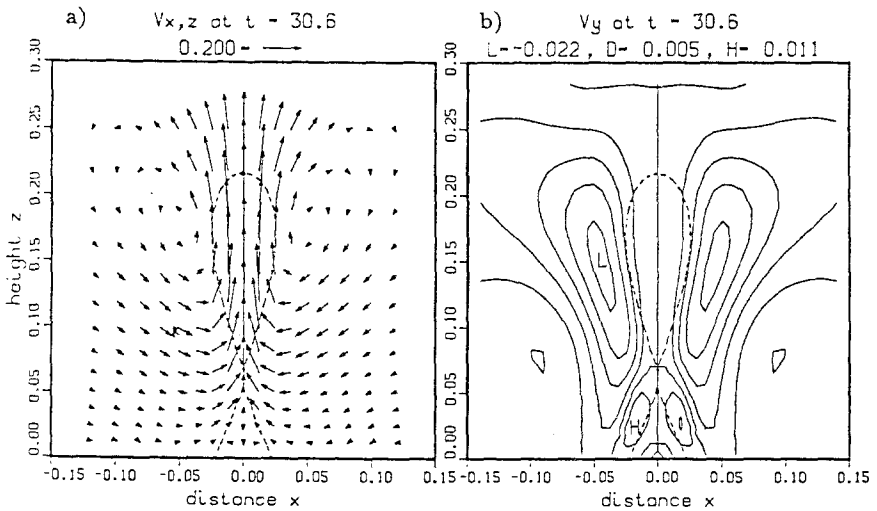

Fig. 6. Velocity field in the x, y-plane (a) and contours of constant v_y (b) at $t = 30.6$, associated with the field represented in the bottom row of Figure 6. The dashed line indicates the separatrix, i.e., the magnetic surface of field lines that pass through the x-line.

A rough estimate of the tearing mode growth time is also in agreement with the rapid evolution after the magnetic diffusivity is switched on. With an Alfvén speed close to unity and a current sheet width of $D = 0.04$, the Alfvén transit time across the current sheet is $\tau_A = D/V_A = 0.04$. The assumed diffusivity in dimensionless units is $\eta = 0.001$ which gives a diffusion time of $\tau_D = D^2/\eta = 1.6$. As a result, the growth time of the tearing mode turns out to be $\sqrt{\tau_A \tau_D} = 0.25$ so that the bottom row of Figure 5 represents the field after somewhat more than two linear growth times.

Note that while the poloidal field evolves to small scales in the vicinity of the x-line, B_y is of order unity all over the reconnection region. As a consequence, the poloidal and

toroidal field diffuse differently, so that B_y cannot be maintained constant along those field lines that intercept the diffusion region. The resulting field-aligned gradients of B_y then lead, according to (1b), to an acceleration of the plasma in the y-direction. Figure 6(b) displays the resulting flow, which is concentrated more or less on the magnetic separatrix defined by those field lines that pass the vicinity of the magnetic x-line. Both, the magnetic and the velocity field therefore have essential y-components in our case and the overall topology, even though it is only two-dimensional, ties in closely with the concepts of general, finite-B reconnection developed recently by Schindler, Hesse, and Birn (1988) and Hesse and Schindler (1988).

4. Nonlinear Evolution

The results of run B, discussed in the previous section, have shown that a transition from a stable to a resistively unstable regime can be achieved by a combination of shear and converging photospheric motions. As this change is obtained within the constraints of ideal MHD, the onset of the instability requires the occurrence of an anomalous resistivity, perhaps generated by a microinstability. On the other hand, the initial configuration, and subsequently the early stages of the evolving configuration, are found resistively stable. It, therefore, seems possible that the resistively unstable regime could be reached even if some resitivity were present during the entire evolution. To investigate this possibility, we performed run C with the same parameters, in particular the same photospheric boundary velocity, as for run B, except that a finite magnetic diffusivity $\eta = 0.001$, or correspondingly $S_m = 1000$, was assumed right from the beginning of the run. Figure 7 displays the projected field lines at various times of the evolution. The instability sets in at about $t \simeq 25$, when a magnetic island forms and begins to grow.

Note, that the magnetic diffusivity is present also at the bottom boundary and causes the magnetic field lines to slip slightly relative to the photospheric plasma flow imposed as boundary condition. The velocity difference due to this slippage is approximately (Mikic, Barnes, and Schmack, 1988)

$$v_{\text{slip}} \simeq \frac{\eta}{D} .$$

It is particularly crucial in our case with converging footpoints because D here is a typical scale across the current sheet and decreases exponentially in time as we have seen above. If there was no tearing instability, the field-line motion in the x-direction would eventually be stopped by the magnetic diffusion if v_{slip} becomes as large as the plasma flow in x-direction, i.e., if

$$v_x \simeq v_{\text{slip}} \simeq \eta \exp(w_{x0} t) .$$

For the parameters of run C, this condition would be reached at

$$t \simeq \frac{1}{w_{x0}} \ln\left(\frac{v_x}{\eta}\right) \simeq 40$$

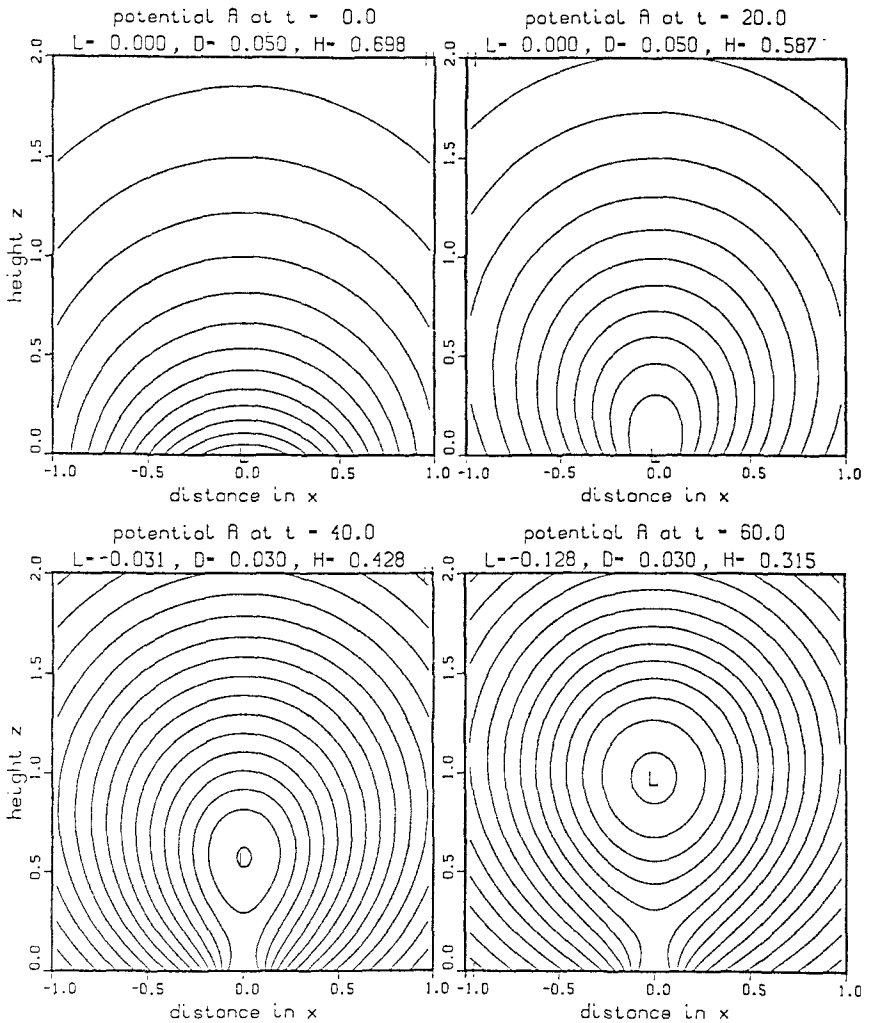

Fig. 7. Field lines projected into the x, z-plane for run C. The parameters are the same as for run B except for S_m which has a value of 1000. The poloidal magnetic flux per unit distance in the y-direction in between a pair of field lines plotted in the figure is $\Delta A = 0.05$ in the dimensionless units for $t = 0$ and 20, and $\Delta A = 0.03$ for $t = 40$ and 60.

for a typical magnitude of the convergent velocity v_x of 0.01 dimensionless units. As the tearing mode sets in already at $t \simeq 25$, the effect of a field-line slippage in the photosphere probably is less critical than the above estimates might suggest.

The plasma dynamics in the vicinity of the reconnection region is no longer controlled by the converging footpoint motion, but is primarily governed by the evolution of the tearing instability. In Figure 8, v_x is plotted along a horizontal line through the x-line at various times after the onset of the instability. The figure shows that the plasma flow velocity towards the x-line grows considerably beyond the speed with which the footpoints are forced to move towards the photospheric neutral line (dashed line in

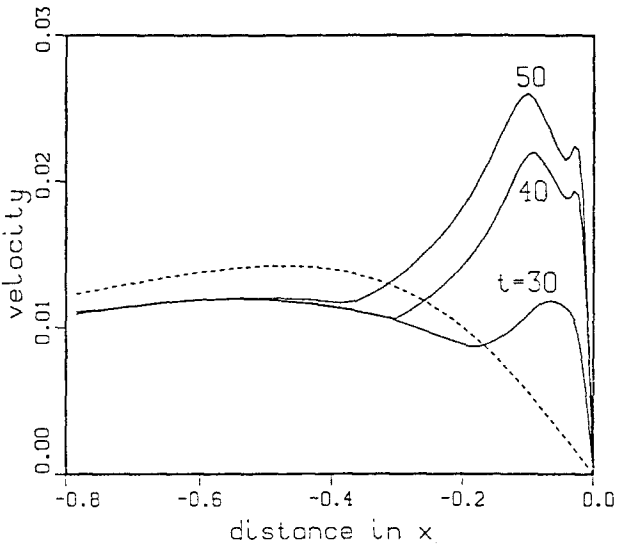

Fig. 8. Velocity component v_x for run C along a horizontal line in the x-direction at the height of the x-line, at various times after instability onset. The dashed line shows, for comparison, v_x at $z = 0$, i.e., the convergent velocity component of the footpoint motion.

Figure 8). The instability which is indirectly brought about by the slow convergence of the footpoints, obviously accelerates the plasma towards the x-line independently from the footpoint motion. In Figure 9, we show the full velocity field obtained when a quasi-stationary reconnection state is reached. From the x-line, the plasma is accelerated upwards to velocities of $0.088 V_{A0}$. At the center of the magnetic island

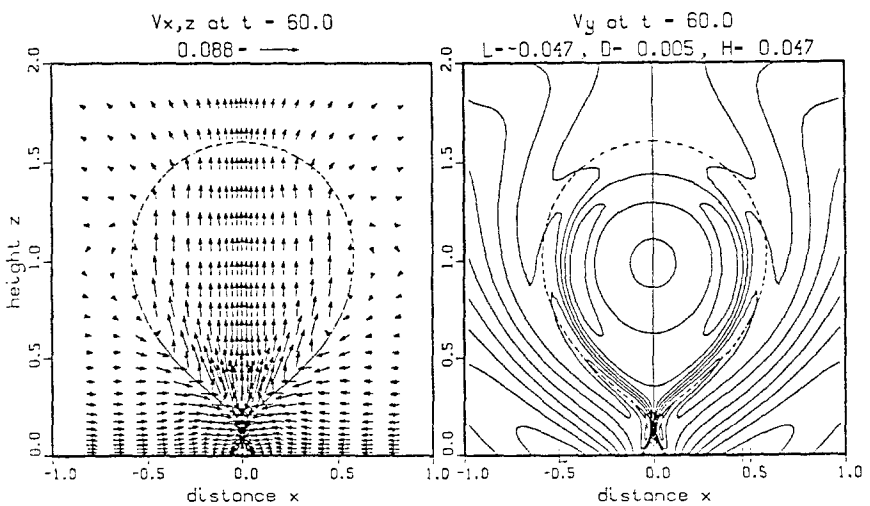

Fig. 9. Velocity vectors in the x, z-plane and contour lines of v_y for run C at $t = 60$. The dashed line indicates the separatrix field line. The difference of the value of v_y between two contour lines is $\Delta v_y = 0.005$.

(drawn dashed in Figure 9), however, the upward velocity has already declined again to about $0.02–0.03 V_{A0}$. Note also the enhancement of v_y on the surface of the magnetic island due to reasons discussed in the previous section.

The tearing instability changes the magnetic topology by creating a pair of x- and o-lines. In the presence of a finite B_y, the o-line becomes the center of a helically twisted flux tube lying horizontally above the photosphere. The field lines that intercept the x-line constitute the separatrix surface, part of which forms the surface of the flux tube. Figure 10 sketches a field line immediately before and after the reconnection process,

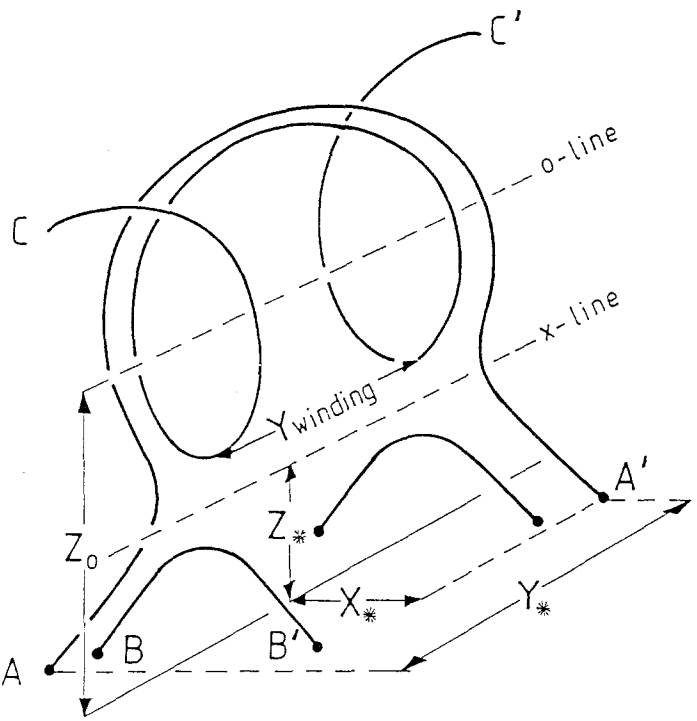

Fig. 10. Approximate geometry of a field line immediately before it is reconnected ($A - A'$) and its fragments after the reconnection ($B - B'$) and ($C - C'$). The reconnection occurs along the x-line and the closed field lines ($C - C'$) are twisted on a magnetic surface around the o-line.

as it is selfconsistently modelled in our simulation. A similar reconnection geometry has been qualitatively proposed by Pneumann (1983) and by van Ballegooijen and Martens (1989). A field line ($A - A'$) that is convected towards the separatrix surface forms after the reconnection process part of a helical field line ($C - C'$) and of the small loops ($B - B'$) underneath the flux tube.

The figure also defines some geometrical distances, the temporal evolution of which we shall investigate in the following. We denote by $A_*(t)$ the value of the magnetic flux function A on the field line that is just about to undergo reconnection at a given time t. Then the contour line $A(x, z, t) = A_*(t)$ represents the separatrix in the x, z-plane and

it intercepts the photosphere at $x = \pm X_*$. The total shear displacement of a field line with its footpoints at $\pm X_*$ at time t is denoted by Y_* and is determined from integrating (4) in time. It could be looked upon as the shear of a field line immediately before it is reconnected. Figures 11(a) and 11(b) show the time development of these two quantities:

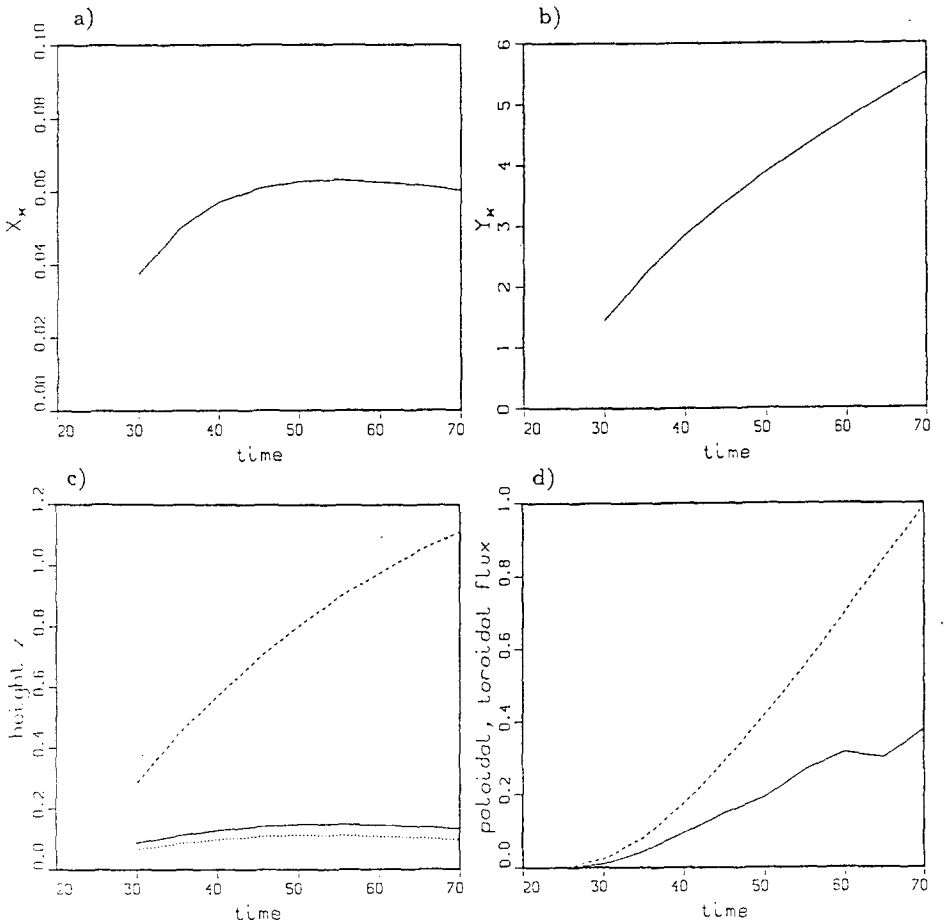

Fig. 11. Time variation of X_* (a), Y_* (b), Z_* (c, solid) and Z_0 (c, dashed) as defined in Figure 10. The dotted line in (c) indicates the height of the spatial maximum of j_y. (d) shows the poloidal flux per unit distance in the y-direction $\Delta A_{\text{fluxtube}}$ and the toroidal flux Φ_{fluxtube} of the helical flux tube as function of time in dimensionless units.

X_* remains almost constant after an initial rise to $X_* \simeq 0.06$ while Y_* increases steadily with time. The height Z_* of the x-line as a function of time is displayed by the solid curve in Figure 11(c). It stays more or less constant at a height of about 0.1 dimensionless units while the height Z_0 of the center of the helical flux tube (dashed curve in Figure 11(c)) continuously rises at roughly 0.02 times the Alfvén speed. This velocity is compatible with the upward plasma velocity shown in Figure 9. Note that the current

density j_y (dotted curve in Figure 11(c)) assumes its maximum always slightly below the magnetic x-line, probably because of the asymmetry imposed onto the tearing mode by the presence of the photosphere. From the x-line, the plasma can be freely accelerated only in the upward direction but not downwards, where the photosphere stops any plasma flow. The downward velocities below the x-line that we obtain in our calculation are smaller than the inflow velocities towards the x-line and we find no signature of a shock system below the reconnection region as invoked by Kopp and Pneumann (1976).

In Figure 11(d) we show the poloidal flux per unit distance in the y-direction, $\Delta A_{\text{fluxtube}} = A_* - A(x = 0, z = Z_0)$ of the helical flux tube (solid curve) and the toroidal flux in the y-direction $\Phi_{\text{fluxtube}} = \int_{A<A_*} B_y \, dx \, dz$ where the integration is over the flux tube area. Both quantities grow after some initial stage almost linearly with time. In particular, the reconnection rate $d/dt(\Delta A_{\text{fluxtube}})$ assumes an approximately constant value after $t \geq 40$. The reconnection rate, on the other hand, has to coincide with the poloidal flux transported through the separatrix surface at the photosphere by the footpoint motion in the x-direction:

$$\frac{d}{dt}(\Delta A_{\text{fluxtube}}) = (B_z v_x)(x = X_*, z = 0) \equiv \frac{d}{dt}(\Delta A_{\text{photosphere}}) . \tag{9}$$

The transport of poloidal flux in the photosphere, however, is completely controlled by the initial and boundary conditions of our model. For small x, both $B_z(x, z = 0)$ and $v_x(x, z = 0)$ are proportional to x so that the right-hand side of Equation (9) becomes proportional to X_*^2. The magnetic field geometry therefore may adjust itself to the reconnection rate by adopting an appropriate value for the separatrix footpoint coordinate X_*. Obviously, an increased reconnection rate will yield an increase in X_* as can be observed in run C for $t \leq 40$. For later times, the constant value observed for X_* is a consequence of the stationarity of the reconnection rate.

Another important quantity linked with the stability of the helical flux tube is the field-line twist of the nested magnetic surfaces that are wound around the o-line. This parameter controls the stability of the flux tube with respect to a kink instability and its capability to confine the flux-tube plasma after it has radiatively cooled. To avoid a kink instability, the flux-tube twist must not exceed a certain threshold value (e.g., Hood and Priest, 1981) while a certain amount of twist is necessary in order to prevent cool and dense plasma in the flux tube falling back onto the photosphere (Priest, Hood, and Anzer, 1989). Both of these effects, however, depend on the three-dimensional structure of the flux tube and cannot properly be taken account of in our present model.

Here, we shall express the field-line twist in terms of the winding length

$$Y_{\text{winding}}(A) = B_y(A) \oint_{A = \text{const.}} \frac{dl}{|\nabla A|} , \tag{10}$$

which is the distance in the y-direction for a closed field line to undergo a twist of 2π on the magnetic surface imbedded in the flux tube and specified by the value

A = const. $< A_*$ of the flux function. Note that the integration in (10) becomes singular as the flux function value A approaches A_* so that (10) is useful only on magnetic surfaces well inside the flux tube which are close to an equilibrium. On these field lines, Y_{winding} is equal to the ratio of the infinitesimal toroidal and poloidal flux in between two neighboring magnetic surfaces and is therefore conserved under ideal conditions (van Ballegooijen and Martens, 1989). In Figure 12, the winding length is plotted versus some measure of the distance of the respective magnetic surface from the o-line.

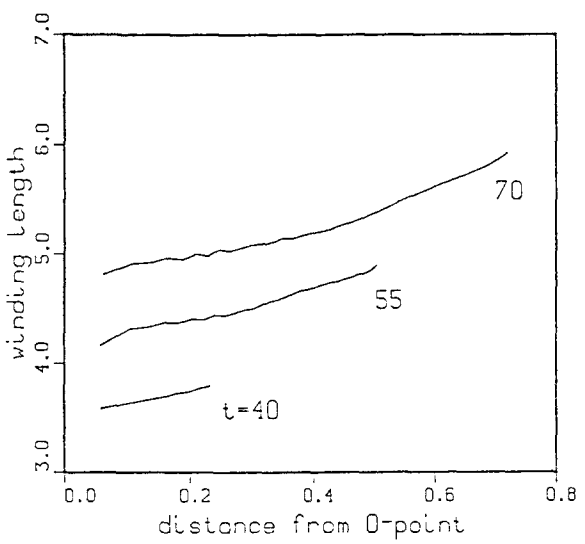

Fig. 12. Winding length Y_{winding} of the flux-tube field lines as a function of the distance between the o-line and the highest point of the field line in z-direction.

Figure 12 shows that Y_{winding} grows with distance from the tube axis and the flux tube is twisted more extensively in its interior and is more relaxed on its outer surfaces. We also see from Figure 12 that Y_{winding} gradually increases in time and is obviously not conserved exactly on each flux tube. This effect is due to the finite diffusivity in our model which causes the flux tube field lines to release their twist and enhance Y_{winding} accordingly. These features indicate that the flux tube becomes more stable as it evolves, so that a possible kink instability should operate in the early stage if at all. We should note, however, that this argument is not conclusive, because the stability properties of a flux tube imbedded in a configuration of line-tied field lines above the tube are certainly different from those of an isolated flux tube.

As another natural consequence of the near-equilibrium structure of the helical flux tube, we find a maximum of the density at the center of the flux tube which is shown in Figure 13. Note that in equilibrium and when the temperature is constant along field lines (which is trivial in our isothermal simulation) the density is inversely proportional to the differential flux tube volume given by (6). For a sheared arcade, we expect $\rho(A)$ to decrease in accord with the discussion in Section 3. Initially, the effect of the shear

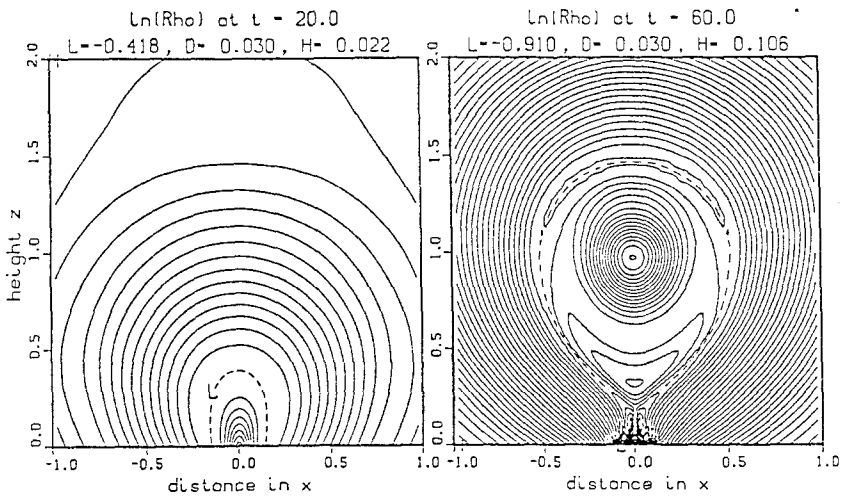

Fig. 13. Contour levels of the density ρ obtained for run C. The dashed line indicates a line of minimum density, $\ln \rho \simeq -0.4$ at $t = 20$ and $\ln \rho \simeq -0.75$ at $t = 60$, respectively. Adjacent contours differ by constant increments in $\ln \rho$, $\Delta (\ln \rho) = 0.03$.

will be to decrease the density by a larger amount the smaller the loop is. In the case of converging footpoint motions, however, compressing tension forces become important and $\rho(A)$ cannot decrease as freely. The tension forces of the poloidal field of the flux tube here cause a local maximum for the density of about $\rho \simeq 0.71$ close to the o-line while a minimum of the density of $\rho \simeq 0.47$ is obtained at $t = 60$ just inside the separatrix. Note that the beginning of this evolution is already visible at $t = 20$, well before the onset of the instability.

5. Summary and Discussion

On the basis of time-dependent, resistive and nonresistive MHD simulations, we have studied the evolution of two-dimensional coronal arcade structures under the influence of plasma motions at the photospheric boundary. These motions lead to a deformation of the magnetic field structure above the photosphere through the effect of line-tying on the magnetic field lines. The motions at the boundary included components both parallel and perpendicular to the axis of the arcade structure. On the Sun, the motion of the magnetic footpoints is forced by the convection of the massive and highly conducting plasma underneath the photosphere. It is therefore quite natural to expect a divergence $(\partial v_x/\partial x + \partial v_y/\partial y)\,(z = 0) \neq 0$ of the photospheric surface velocity. Note, however, that due to the boundary conditions that we have chosen, there is no flux cancellation in the photosphere, i.e., B_z integrated over the photospheric half plane to the right or the left of the neutral line remains a constant. Our boundary conditions also exclude an emergence or a submergence of magnetic flux as proposed by Priest (1990) since we assume $v_z = 0$ in the photospheric plane.

For the example studied we found that a photospheric shear motion, parallel to the axis of the arcade structure, leads to an evolution in which the instantaneous configuration stays close to a force-free equilibrium, $\mathbf{j} = \alpha\mathbf{B}$, with a uniform ratio α between $\mathbf{j}$ and $\mathbf{B}$. Such an equilibrium represents the minimum energy state for the given boundary conditions with prescribed helicity and thus indicates its stability. No loss of equilibrium was found either for this case, consistent with earlier results on sheared configurations (Klimchuk, Sturrock, and Yang, 1988; Biskamp and Welter, 1989).

The results were altered when a velocity component toward the axis of the arcade structure was added to the photospheric footpoint motion. While, again, no loss of equilibrium was found, the configuration entered a regime which was found to be unstable to a resistive tearing mode. The resistive stability was tested by switching-on a finite resistivity. The tearing/reconnection regime could also be entered when finite resistivity was present during the entire evolution.

The key to the tearing mode that develops due to the footpoint motion seems to be the formation of a thin current sheet. As we showed in Section 3, the width of the current sheet decreases almost exponentially as $D \simeq \exp(-w_{x0}t)$, where $w_{x0} = -\partial v_x/\partial x$ at $x = z = 0$, and accordingly the momentary tearing-mode growth time varies as $\sqrt{\tau_A \tau_D} \simeq D^{3/2}\eta^{-1}$. To a first approximation, we expect the instability to start if $\sqrt{\tau_A \tau_D}$ becomes sufficiently small so that the time of the instability onset scales with the magnetic diffusivity and with the converging footpoint velocity as $t \sim \ln(\eta)/w_{x0}$.

The formation of a current sheet in our model bears some resemblance to the development of tangential discontinuities proposed by Parker (1972) as a heating mechanism of the coronal plasma. Even though the photospheric velocity is smooth, the line-tied magnetic structures evolve such that exponentially decreasing scales are produced. In our case, however, the divergence $(\partial v_x/\partial x + \partial v_y/\partial y)\,(z = 0) \neq 0$ of the photospheric boundary velocity plays a decisive role, while Parker (1972) explicitly considers a non-divergent footpoint motion.

It has long been argued, based on solutions of the stationary problem (3b) obtained with the generating function method, that a two-dimensional arcade may loose its equilibrium if the toroidal magnetic field B_y, or likewise the toroidal current j_y can be enhanced sufficiently (Jockers, 1976, 1978; Birn, Goldstein, and Schindler, 1978; Birn and Schindler, 1981; Low, 1977, 1982; and others). In this method, $B_y^2/2 + p$ in (3b) is expressed as $\lambda F(A)$ where the functional form of $F(A)$ is assumed to remain invariant and λ is varied so that a continuous family of solutions of (3b) is obtained. If we again neglect the small plasma pressure for simplicity, λ controls the magnitude of B_y. The existence of a critical value for the magnitude parameter λ, beyond which solutions to (3b) could not be found, was taken as evidence for the existence of a nonequilibrium once B_y exceeds a certain threshold. As we found in Section 3, however, in the structures considered, B_y cannot be enhanced to an arbitrary magnitude by a shear of the footpoints alone, but a convergent component of the footpoint motion may lead to a continuous increase of B_y and j_y. The consideration of a converging footpoint motion may provide a connection to earlier work that has utilized the generating function method. A formal connection can be established by assuming a footpoint motion as in

(7) and by introducing new coordinates $x' = x \exp(w_{x0}t)$, $z' = z \exp(w_{x0}t)$ according to (8). In these transformed coordinates there is no more converging motion of the field-line footpoints. The problem of finding a sequence of equilibria that satisfy (3b) then relates to a similar problem without converging motion in the new coordinates with

$$\Delta' A = -e^{-2w_{x0}t} B_y \frac{\partial}{\partial A} B_y ,$$

where Δ' is the Laplace operator with respect to the new coordinates and the small thermal pressure is again neglected for simplicity. If $B_y(A)$ is fixed, then the flux function A in the new coordinate system more and more approaches a potential field because the converging motion enhances the gradient $\nabla' A$ with respect to the new coordinates over B_y. If, however, we assume instead the shear-displacement $Y(A)$ of the field lines is fixed, we also have to rescale B_y:

$$B_y(A) = Y(A)\left(\int_{-}^{+} \frac{\mathrm{d}l}{|\nabla A|} \right)^{-1} =$$

$$= Y(A) e^{2w_{x0}t} \left(\int_{-}^{+} \frac{\mathrm{d}l'}{|\nabla' A|} \right)^{-1} = e^{2w_{x0}t} B'_y(A) ,$$

in order to conserve the magnetic flux in the y-direction. This finally gives

$$\Delta' A = -e^{2w_{x0}t} B'_y \frac{\partial}{\partial A} B'_y \tag{11}$$

instead of (3b). In accordance with the references given above, critical values for the parameter $\lambda = \exp(2w_{x0}t)$ exist for certain functional forms of $B'_y(A)$, beyond which a solution to (11) does not exist. The critical parameter value here relates to a critical time after the beginning of the converging footpoint motion. However, the analogy cannot be drawn too far: we found in Section 3 that $B_y(A)$ does not evolve self-similarly if the footpoints converge but changes its functional form, which contradicts the assumption of an invariant $B_y(A)$ made in the generating function approach. Our simulations thus could not demonstrate that a cessation of equilibrium can be forced by footpoint motions, whereas the transition into a resistively unstable regime was clearly demonstrated.

After the instability has set in, a helical flux tube is formed and a more or less quasi-stationary state arises with a constant reconnection rate and a linear increase of the magnetic flux trapped in the flux tube. It turns out that the convergent component of the footpoint motion besides controlling the time for the onset of the instability seems to determine the distance X_* between the photospheric neutral line and the footpoint of those field lines that go through the magnetic x-line underneath the flux tube. As one expects the field lines connected to the x-line to be heated by the dissipation in the

diffusion zone around the x-line, their footpoints could be the site of enhanced Hα luminosity. The distance between the Hα-ribbons thus formed on either side of the photospheric neutral line should then be $2X_*$ and should stay almost constant in time during the quasi-stationary phase of the evolution.

The shear component of the footpoint motion, on the other hand, controls the twist of the helical flux tube and thereby its stability with respect to a kink instability. The relation between the shear and the flux tube twist causes the twist to decrease with distance from the center of the tube. If therefore the shear is so large as to produce a kink instability of the flux tube, this will already occur when the flux tube is still thin. Conversely, if the flux tube is stable initially, it will probably remain so during the quasi-stationary phase. In order to find out how close the flux tube formed by the tearing mode is to a kink instability, we intend to perform three-dimensional simulations of the model investigated here.

Another potential shortcoming of the present calculations is the neglect of gravity and a proper energy balance. The gravity term in (1b), if normalized like the other terms, would be $(\beta_0 L_0/H_0)\rho$ where H_0 denotes the according atmospheric pressure scale height. Compared to the pressure term in (1b), the gravity term is negligible if the vertical scale of the density variation in our model does not exceed H_0, which in the corona has a typical value of 50 000 km (Priest, 1982). Preliminary calculations which include a gravity term with an initial density variation of $\rho_0 \exp(-z)$ do not show essential differences from the results presented here, even for a ratio $H_0/L_0 = 1$.

Our model calculation is far too simple to represent a specific active solar phenomenon in greater detail. The present work bears considerable resemblance and was in fact motivated by the model for the formation of solar prominences proposed by van Ballegooijen and Martens (1989). In our view, however, the virtue of the present calculations leads beyond this specific mechanism. They prove that thermal energy sources are not necessary to drive a simple, initially stable magnetic field configuration towards an instability and that this can be achieved by line-tied motions alone. According to the spatial scale that we assume, the processes considered here may serve as a basis for the formation of a filament or the generation of flares and nanoflares. Concerning the formation of a filament, an interesting result of our simulation is the natural enhancement of the density inside the flux tube that after cooling could constitute the dense filament plasma.

Acknowledgements

One of the authors (B.I.) would like to thank the Space Physics group of LANL and especially its leader S. P. Gary for the hospitality he experienced during his stay in Los Alamos. Los Alamos portions of this work were supported by the U.S. Department of Energy through the Office of Basic Energy Sciences and by NASA.

References

Berger, M. A.: 1984, *Geophys. Astrophys. Fluid Dynamics* **30**, 79.

Birn, J. and Schindler, K.: 1981, in E. R. Priest (ed.), *Solar Flare Magnetohydrodynamics*, Chapter 6, Gordon and Breach, London.

Birn, J., Goldstein, H., and Schindler, K.: 1978, *Solar Phys.* **57**, 81.

Biskamp, D. and Wezlter, H.: 1989, *Solar Phys.* **120**, 49.

Forbes, T. G.: 1990, *J. Geophys. Res.* **95**, 11919.

Forbes, T. G. and Priest, E. R.: 1983, *Solar Phys.* **84**, 169.

Furth, H. P., Killeen, J., and Rosenbluth, M. N.: 1963, *Phys. Fluids* **6**, 459.

Golub, L., Maxson, C., Rosner, R., Serio, S., and Vaiana, G. S.: 1980, *Astrophys. J.* **238**, 343.

Hesse, M. and Schindler, K.: 1988, *J. Geophys. Res.* **93**, 5559.

Hood, A. W. and Priest, E. R.: 1981, *Geophys. Astrophys. Fluid Dynamics* **17**, 297.

Howard, R. A., Sheeley, N. R., Koomen, M. J., and Michels, D. J.: 1985, *J. Geophys. Res.* **90**, 8173.

Jockers, K.: 1976, *Solar Phys.* **50**, 405.

Jockers, K.: 1978, *Solar Phys.* **56**, 37.

Klimchuk, J. A., Sturrock, P. A., and Yang, W.-H.: 1988, *Astrophys. J.* **335**, 456.

Kopp, R. A. and Pneumann, G. W.: 1976, *Solar Phys.* **50**, 85.

Linker, J. A., van Hoven, G., and Schnack, D. D.: 1990, *J. Geophys. Res.* **95**, 4229.

Low, B. C.: 1977, *Astrophys. J.* **212**, 234.

Low, B. C.: 1982, *Rev. Geophys. Space Phys.* **20**, 145.

Mikic, Z., Barnes, D. C., and Schnack, D. D.: 1988, *Astrophys. J.* **328**, 830.

Parker, E. N.: 1972, *Astrophys. J.* **174**, 499.

Parker, E. N.: 1983, *Astrophys. J.* **264**, 642.

Pneumann, G. W.: 1983, *Solar Phys.* **88**, 219.

Priest, E. R.: 1982, *Solar Magnetohydrodynamics*, D. Reidel Publ. Co., Dordrecht, Holland.

Priest, E. R.: 1990, in E. R. Priest and V. Krishan (eds.), 'Magnetic Reconnection on the Sun', *IAU Symp.* **142**.

Priest, E. R., Hood, A. W., and Anzer U.: 1989, *Astrophys. J.* **344**, 1010.

Sakurai, T.: 1979, *Publ. Astron. Soc. Japan* **31**, 209.

Sakurai, T.: 1989, *Solar Phys.* **121**, 347.

Schindler, K., Hesse, M., and Birn, J.: 1988, *J. Geophys. Res.* **93**, 5547.

Steinolfson, R. S. and Hundhausen, A. J.: 1988, *J. Geophys. Res.* **93**, 14,269.

Van Ballegooijen, A. A. and Martens, P. C. H.: 1989, *Astrophys. J.* **343**, 971.

White, R. B.: 1983, in M. N. Rosenbluth and R. Z. Sagdeev (eds.), *Handbook of Plasma Physics*, Vol. 1: A. A. Galeev and R. N. Sudan (eds.), Basic Plasma Physics I, Chapter 3.5, North-Holland Publ. Co., New York.

Woltjer, L.: 1958, *Proc. Nat. Acad. Sci. USA* **44**, 489.

Zwingmann, W.: 1987, *Solar Phys.* **111**, 309.